Functional renormalization group for the anisotropic triangular antiferromagnet

Johannes Reuther[1] and Ronny Thomale[2]

[1]*Institut für Theorie der Kondensierten Materie, Karlsruhe Institute of Technology, D-76128 Karlsruhe, Germany*

[2]*Department of Physics, Princeton University, Princeton, New Jersey 08544, USA*

(Received 14 October 2010; revised manuscript received 11 November 2010; published 4 January 2011)

We present a functional renormalization group scheme that allows us to calculate frustrated magnetic systems of arbitrary lattice geometry beyond $O(200)$ sites from first principles. We study the magnetic susceptibility of the antiferromagnetic (AFM) spin-1/2 Heisenberg model ground state on the spatially anisotropic triangular lattice, where J' denotes the coupling strength of the intrachain bonds along one lattice direction and J the coupling strength of the interchain bonds. We identify three distinct phases of the Heisenberg model. Increasing $\xi = J'/J$ from the effective square lattice $\xi = 0$, we find an AFM Néel order to spiral order transition at $\xi_{c1} \sim 0.6$–0.7, with an indication that it is of second order. In addition, above the isotropic point at $\xi_{c2} \sim 1.1$, we find a first-order transition to a magnetically disordered phase with collinear AFM stripe fluctuations.

DOI: 10.1103/PhysRevB.83.024402 PACS number(s): 75.10.Jm, 75.30.Kz, 75.50.Ee

I. INTRODUCTION

Frustration induced by lattice geometry and interaction in two-dimensional quantum antiferromagnets constitutes a considerable challenge beyond mean-field theory.[1] This is the main reason why the question of distinguishing systems with magnetic long-range order and spin liquid behavior has been one of the most difficult and long-standing problems in the field of quantum magnetism. A plethora of different methods has been developed to address this problem in the context of many different lattices and magnetic Hamiltonians. Analytical perturbative and semiclassical approaches all share the deficiency that they generally tend to underestimate quantum fluctuations affecting magnetic order. This is essentially because, at zero temperature in two dimensions, only magnetically ordered quantum phases possess classical analogues, while the notion of a magnetically disordered system is a pure quantum effect. Various numerical methods have been applied to this type of problem, most of which, however, have severe drawbacks of very different kinds. Quantum Monte Carlo (QMC) methods[2] may suffer from the sign problem often encountered for frustrated systems, while exact diagonalization (ED) studies are constrained to small system sizes. Conventional density matrix renormalization group (DMRG) methods[3,4] partly resolve the latter problem, but they are constrained to (effectively) one-dimensional systems. Coupled cluster methods (CCM)[5] and variational QMC methods[6] are valuable approaches to treat frustrated two-dimensional systems. However, while they do not suffer from insufficient system size, they are limited in the sense that, generally, only trial state energies can be tested against each other, and no unbiased treatment from first principles is possible.

Promising lines of improvement have been undertaken recently. In special cases where it is applicable, dimer projection schemes allow the treatment of larger systems at a similar level of precision and completeness to ED.[7] From a perturbative expansion perspective, continuous unitary transformation (CUT) methods provide a helpful tool to compute the energies of the ground state and excitation modes of small quasiparticle sectors.[8,9] Adapted DMRG algorithms have also been extended to two-dimensional geometries, in applications to both bipartite and nonbipartite lattices.[10] However, in particular in the strongly frustrated cases, the finite size and discarded entropy weight scalings are very challenging, limiting its application to larger system sizes.

Furthermore, the generalized notion of matrix product states, in certain cases, leads to an efficient treatment of two-dimensional magnetic systems by projected entangled pair states (PEPS).[11] In particular, the multiscale entanglement renormalization ansatz (MERA) provides a new tool to compute energies and scaling behavior of certain magnetic systems and has been most recently applied to frustrated systems.[12,13] Still, even in the optimal cases where the approximations made within these methods are controlled, it is mainly suited to determine certain ground-state properties only. For frustrated magnetic systems and actual comparison to experiment, however, it would be most desirable to compute complementary thermodynamic quantities that allow us to resolve the competition and classification of magnetic ordering and quantum fluctuations. The most suitable quantity in this respect is the magnetic susceptibility. Interpreted as the magnon spectral function, it provides detailed information about the qualitative and quantitative type of magnetic fluctuations, and it is the canonic quantity measured in experiment. In this paper, we employ the pseudofermion functional renormalization group (PFFRG)[14] as a method to tackle systems of frustrated magnetism. Applying the method to the anisotropic triangular lattice, we demonstrate that the PFFRG (i) is able to treat large system sizes of $O(200)$ sites, (ii) is applicable to arbitrary frustrated lattice geometries and two-body bare interactions, (iii) naturally allows us to compute the magnetic susceptibility as the canonical outcome of the renormalization group (RG), and (iv) hence provides an unbiased calculation from first principles that allows comparison to experiment.

The paper is organized as follows. In Sec. II, we introduce the Heisenberg model on the anisotropic triangular lattice and elaborate on previous works and experimental realizations associated with it. In Sec. III, we give a brief introduction to a functional renormalization group formulation of spin systems reported on previously.[14] In particular, we classify which

diagrammatic subsets summed over within our method account for magnetic ordering and disordering tendencies, assuring that our method treats all fluctuations on the same footing. In Sec. IV, we report our results on the magnetic susceptibility for the anisotropic triangular lattice. For the anisotropy parameter $\xi < 1$ we specifically discuss the antiferromagnetic (AFM) Néel to 120° Néel order transition, which we find to be of second order with no magnetically disordered phases in between and with a transition value $\xi \sim 0.6$–0.7 which is shifted upward as compared to the classical solution due to quantum fluctuations. For weak anisotropy $\xi \sim 1.1$, we observe a first-order transition into a magnetically disordered phase. From the magnetic susceptibility, however, we can still obtain the magnetic fluctuation properties of this phase, which we find to smoothly evolve into collinear AFM type. In Sec. V, we conclude that our slave particle (pseudofermion) functional renormalization group method establishes a promising approach to adequately describe the interplay of magnetic order and disorder in frustrated magnets.

II. MODEL

The Heisenberg model on the anisotropic triangular lattice (ATLHM) attracted considerable attention in recent years as an experimentally accessible testing ground for quantum magnetism disorder phenomena. The Hamiltonian is given as

$$H_{\mathrm{ATLHM}} = J \sum_{\langle i,j\rangle_{\mathrm{V}}} \vec{S}_i \vec{S}_j + J' \sum_{\langle i,j\rangle_{-}} \vec{S}_i \vec{S}_j, \qquad (1)$$

where the coupling J' applies to the bonds along (horizontal) one-dimensional chains and J is the coupling between them, forming a triangular lattice altogether [Fig. 1(a)]. We define $\xi = J'/J$ as a parameter to interpolate between the effective square lattice limit $\xi = 0$ and the disordered isolated chain limit $\xi \to \infty$. Experiments on Cs_2CuCl_4 ($\xi \sim 2.94$) provide an excellent testing ground of discussing various features of spin liquid behavior.[15] (Influences such as Dzyaloshinskij-Moriya interactions complicate the experimental picture.) The formation of a magnetically ordered state for smaller ξ opposed to disorder tendencies for larger ξ can be nicely studied for the organic $\kappa - (\mathrm{BEDT-TTF})_2\mathrm{X}$ family. While $\mathrm{X} = \mathrm{Cu_2N(CN)_2]Cl}$ shows an AFM transition of $T_{\mathrm{N}} = 27$ K with

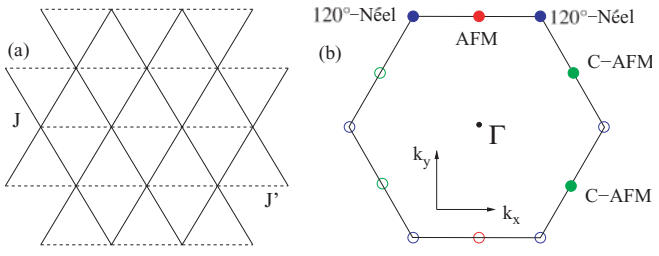

FIG. 1. (Color online) (a) Triangular lattice structure. The horizontal bonds correspond to coupling J' and the others to coupling J. (b) Schematic plot of the hexagonal Brillouin zone. Different magnetic order resides at different points [AFM Néel order, 120° Néel order, collinear AFM order (c-AFM)]. The open circles relate to the filled circles by reciprocal lattice vectors, i.e., AFM order corresponds to two points in the Brillouin zone, collinear AFM to four points, and 120° Néel order to six points.

estimated $\xi = 0.55$, the $\mathrm{X} = \mathrm{Cu_2(CN)_3}$ compound, estimated to be nearby the symmetric triangular regime $\xi = 1.15$, does not show magnetic order down to very low temperatures.[16] Similar findings are obtained[17] for $\mathrm{EtMe_3Sb[Pd(dmit)_2]_2}$, which is located around $\xi = 1.1$. Details of the phase diagram of (1) are still currently debated. It is an established fact that the system is AFM Néel-ordered for small ξ, changing to 120° Néel order as the isotropic triangular limit $\xi = 1$ is reached.[18–24] However, different methods provide differing indication about the nature and position of the transition between those phases: An intermediate disordered phase has been proposed in the literature,[25] while in other works a direct transition is assumed, but the transition cannot be classified to be of second or first order.[22,23] For larger $\xi > 1$, some works indicate a disordered phase extending to the $\xi \to \infty$ limit,[20,26] whereas others indicate collinear antiferromagnetic (c-AFM) ordering.[23,24,27]

III. PSEUDOFERMION FUNCTIONAL RENORMALIZATION GROUP

We now address this problem with PFFRG, which is explained in more detail in Ref. 14. Unlike conventional functional renormalization group (FRG) studies, our starting point is not given by the bare excitations of the system. Instead we use the pseudofermion representation of spin-1/2 operators $S^{\mu} = 1/2 \sum_{\alpha\beta} f^{\dagger}_{\alpha} \sigma^{\mu}_{\alpha\beta} f_{\beta}$, $(\alpha,\beta = \uparrow,\downarrow,\ \mu = x,y,z)$ with the fermionic operators $f_{\uparrow}$ and $f_{\downarrow}$ and the Pauli matrices σ^{μ}. This representation enables us to apply the methods of quantum field theory (Wick's theorem), leading to standard Feynman many-body techniques. The introduction of pseudofermions comes along with an artificial enlargement of the Hilbert space and therefore requires the fulfillment of an occupancy constraint (exclusion of empty and doubly occupied states). Since an unphysical occupation acts as a vacancy in the spin lattice associated with an excitation energy of order J, particle number fluctuations are suppressed at zero temperature and the constraint is naturally fulfilled. Quantum spin models are inherently strong coupling models, requiring infinite self-consistent resummations of perturbation theory. In this context FRG[28–31] provides a systematic summation in different interaction channels by generating equations for the evolution of all one-particle irreducible m-particle vertex functions under the flow of an infrared (IR) frequency cutoff Λ [see Figs. 2(a) and 2(b) for the flow of the self-energy and the two-particle vertex]. In order to reduce the infinite hierarchy of equations to a closed set, some truncation scheme has to be applied. As an important difference in the PFFRG as compared to conventional FRG schemes, we still include certain two-loop contributions that are shown by Katanin[32] to be essential for a better fulfillment of Ward identities [see Fig. 2(c)]. In particular, in this way the random-phase approximation (RPA) is recovered as a diagram subset generated by the RG flow.[33] It is important to emphasize that the RPA diagrams play a crucial role in our scheme as they are responsible for the collective ordering phenomena. These graphs can be understood as the leading contribution of a $1/S$ expansion[34,35] (where S is the spin length), favoring magnetic order. In addition, our approximation includes the full particle-particle ladder as well as the particle-hole ladder which presents the leading term in a

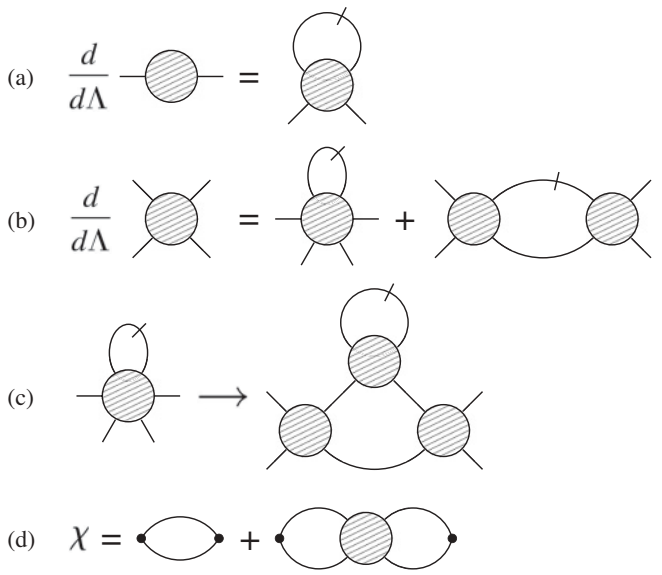

FIG. 2. Graphic representation of the FRG differential equations. Bare lines denote the (renormalized and scale-dependent) Green's functions and slashed lines the single scale propagators. Equations (a) and (b) are the FRG equations for the self-energy and the two-particle vertex, respectively [without distinguishing between the different pairing channels on the right side of (b)]. The Katanin scheme is given by the replacement (c). By fusing the external legs of the two-particle vertex, the magnetic susceptibility is obtained, as shown in (d).

$1/N$ expansion [where N is the dimension of the generalized symmetry group SU(N)]. Paramagnetic quantum phases have been previously described within such an expansion.[36,37] Generally, these graphs favor disorder tendencies. Including both contributions from the $1/S$ and $1/N$ expansion hence enables us to adequately treat the competition of magnetic order and disorder in an unbiased fashion. The magnetic susceptibility can be conveniently computed from the two-particle vertex [Fig. 2(d)]. Due to the local nature of the auxiliary fermions of a bare spin model, a real-space representation of all vertices is much more suitable than the usual momentum-space scheme. Furthermore, since we operate in the strong coupling limit, the proper regularization of Green's functions requires the self-consistent back coupling of the self-energy [Fig. 2(a)] into the propagators in Fig. 2(b). In order to account for the dynamic fluctuations, it is also necessary to keep all frequency dependencies of the vertex functions. The numerical solution requires the discretization of all frequency dependencies. Similarly, the spatial dependence is approximated by keeping correlation functions of an infinite system up to a maximal length. In our calculations, this length extends over seven lattice spacings, leading to a correlation area of 169 lattice sites (which constrains resolvable incommensurable order to vector sizes within that range). An ordering instability is initially signalled by a strong rise of the vertex couplings associated with this order at some finite scale of Λ (Figs. 3 and 5). Since in the present formulation rotational invariance is conserved during the flow, we should not find stable solutions down to $\Lambda = 0$ in magnetically ordered regimes. Indeed, the onset of spontaneous long-range order is signalled by a sudden breakdown of the smooth flow. In contrast, the existence of a stable solution indicates the absence of long-range order.

IV. MAGNETICALLY ORDERED AND DISORDERED PHASES

A. Néel order to spiral order transition

We sweep through the parameter space of ξ from the square lattice to the isotropic triangular lattice and compute the static magnetic susceptibility shown in Fig. 3. [The peak positions for different types of long-range order are depicted in Fig. 1(b).] Throughout this parameter regime, we observe a characteristic breakdown of the flow, indicating ordering instabilities rather than a disordered phase. One can nicely observe how the susceptibility evolves as we increase ξ.

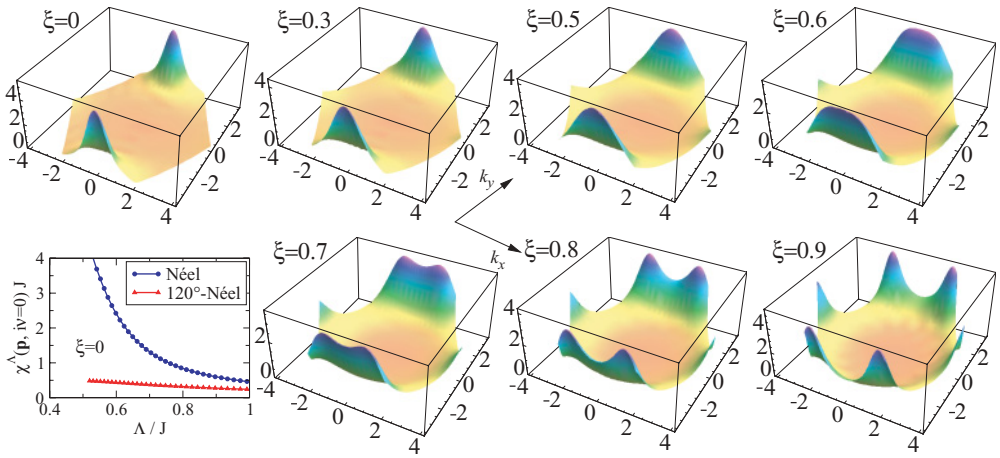

FIG. 3. (Color online) Static magnetic susceptibility resolved for the whole Brillouin zone, by varying $\xi = J'/J$ from the effective square lattice $\xi = 0.0$ close to the triangular lattice $\xi = 0.9$. Bottom Left: Two-particle vertex flow for the AFM Néel channel (blue) versus the 120° Néel channel (red) at $\xi = 0$ with respect to the IR cutoff flow parameter Λ. We observe that the AFM vertices start to diverge, signaling a magnetic instability. Susceptibilities are always given in units of $1/J$. The respective types of order for the distinct peaks positions are shown in Fig. 1(b).

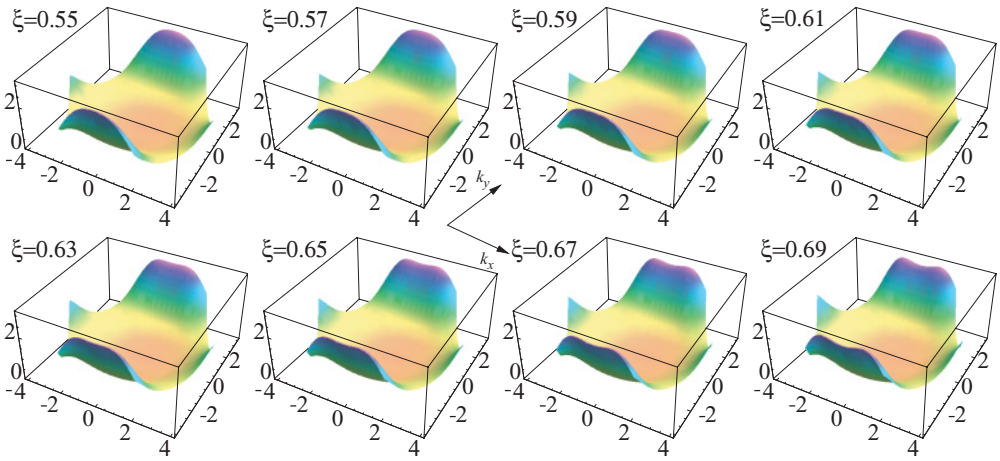

FIG. 4. (Color online) Static magnetic susceptibility, by varying ξ from the AFM Néel side $\xi = 0.55$ across the phase transition to spiral ordering. The already broadened AFM Néel peak splits into two incommensurate peaks that successively shift toward the edges of the Brillouin zone where the 120° Néel order peaks reside.

As shown in Fig. 3, we find a broadening and subsequent splitting of the Néel peak. The split peaks evolve along the Brillouin-zone edge and the weight at the corners of the hexagon increases until in the isotropic case the peak symmetrically resides at the corner position. From the splitting of the Néel peak, we estimate the transition to be at $\xi_{c1} \sim 0.6$–0.7, i.e., the regime above which the order becomes incommensurate. Apparently, the system influenced by quantum fluctuation favors AFM fluctuations over spiral fluctuations, since the classical transition point at $\xi = 0.5$ is shifted to higher ξ.

We have resolved the Néel order to spiral order transition in higher resolution by varying the anisotropy parameter ξ in small step widths (see Fig. 4). We find that the previous Néel peak first broadens along k_x and then smoothly splits into two peaks, which then evolve along the Brillouin-zone boundary. This comes along with increasing spectral weight at the corners of the Brillouin zone. Note that, as a consequence of the periodicity in momentum space, the emerging peak structure at $k_y = 0$ presents the tails of the broadened Néel peak. By increasing ξ further toward the isotropic triangular point the split peaks move toward the corner position until at $\xi = 1$ the hexagonal symmetry of the susceptibility is reached. As the susceptibility evolves completely smoothly through the transition, we find it to be of second order, while an extremely weak first-order transition (corresponding to a slight kink in the leading susceptibility channel) cannot be excluded as a matter of principle. We identify the wave vector of the corresponding long-range-ordered phases with the position of the maximal susceptibility. From this we locate the transition point at such ξ where the peak splits and above which the order becomes incommensurate. From Fig. 4 a transition at $\xi \approx 0.61$ can be read off. In the calculations for this figure we kept correlations up to a length of five lattice spacings (as compared to seven lattice spacings in Figs. 3 and 5). In addition, the number of discrete frequencies has been slightly reduced in Fig. 4. These reductions generally result in lower and broader peaks, which demonstrates that (according to the fact that the phases in

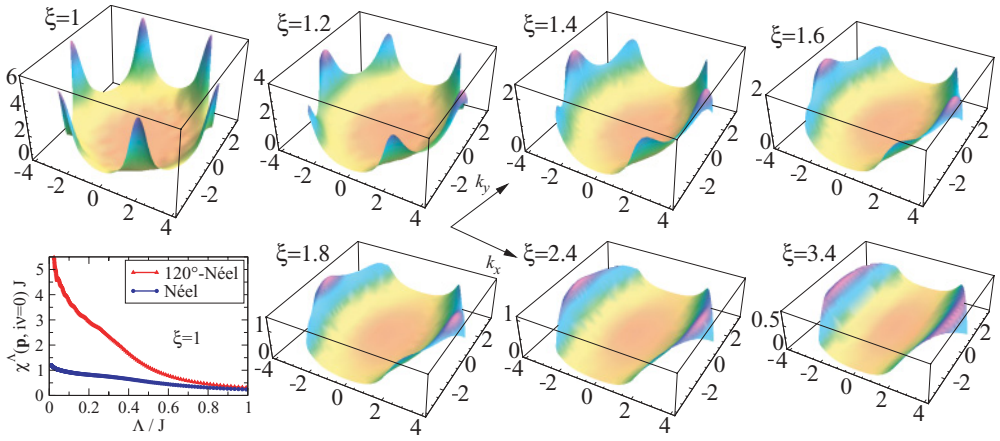

FIG. 5. (Color online) Static magnetic susceptibility, by varying ξ from the isotropic triangular lattice $\xi = 1.0$ toward the one-dimensional chain limit $\xi \to \infty$. Bottom left: Vertex flow at the $\xi = 1$ point. The rise of the 120° Néel channel shows the ordering instability at the isotropic triangle point. Compared to the flow at $\xi = 0$ (Fig. 3), the rise takes place at a much lower scale of Λ, indicating a lower ordering scale for the triangular lattice.

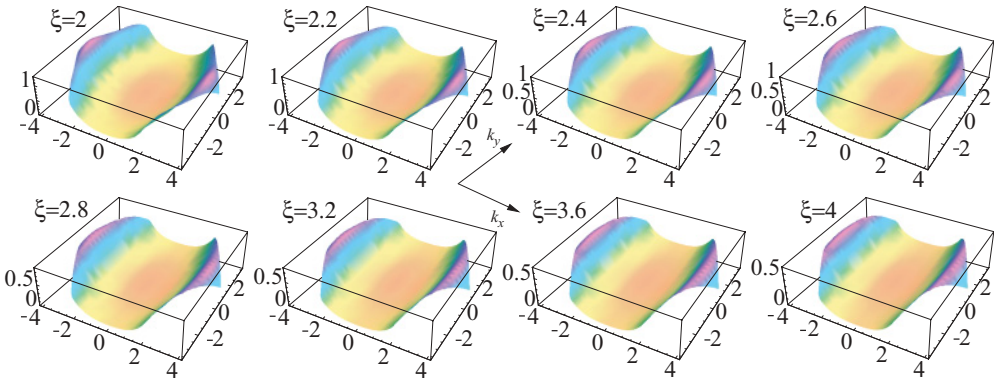

FIG. 6. (Color online) Static magnetic susceptibility, by varying ξ in the strongly anisotropic regime from $\xi = 2$ to $\xi = 4$. While the spectral structure remains rather invariant of c-AFM type, which is strongly smeared along the k_y direction, the total spectral weight slightly decreases with increasing ξ.

this parameter regime are long-range-ordered) there are still finite-size effects in the susceptibility. Another effect seen in a finite-size scaling is that with increasing length of correlations (and also increasing number of discrete frequencies), the transition point moves toward slightly higher ξ. Therefore, from a finite-size scaling we estimate the transition to be approximately centered between $\xi = 0.6$ and $\xi = 0.7$. At the isotropic triangular point $\xi = 1$ where additional lattice symmetries enable us even to consider systems beyond 250 sites, we also obtain higher and sharper peaks with increasing system size.

B. Magnetic disorder transition and collinear antiferromagnetic fluctuations

In a recent work, Starykh and Balents have found that, for $\xi > 1$, the quantum system enters a collinear antiferromagnetic stripe phase.[27] This is interesting since the classical estimate would be spiral order in that regime, so the quantum fluctuations lead to a different ordering.[24] However, finite-size numerical studies have revealed a disordered phase in that regime.[22] Our results for the magnetic susceptibility for $\xi \geqslant 1$ are shown in Fig. 5. As depicted, we observe a strong drop in the magnetic susceptibility above the isotropic point, i.e., in the regime $\xi_{c2} \gtrsim 1.1$. From here, no ordering instability is found in the RG flow and the susceptibility rapidly loses the 120° Néel order signature. While the 120° Néel order peaks die out quickly, AFM stripe fluctuation signatures emerge (at points of the Brillouin zone according to Fig. 1). The transition appears to be of first order according to a pronounced kink in the maximal susceptibility upon varying ξ. While we do not find a breakdown of the flow that would indicate magnetic ordering, we still obtain strong collinear AFM stripe fluctuations (in agreement with Ref. 27) signalled by an unstable RG flow that develops oscillations sensitively depending on the frequency discretization. These fluctuation tendencies are also seen at higher ξ where the peak structure is still visible along the k_x direction. However, these peaks are strongly broadened along the k_y axis, i.e., smeared between the two c-AFM ordering vector positions. This indicates a fast exponential decay of spin correlations between the J' chains. There are proposals in the literature that the (supposedly) disordered regime splits into two (gapped or gapless) different spin liquid phases.[26] In principle this would correspond to a change of diffuse spectral weight in the magnetic susceptibility going from an ungapped to a gapped system. In general, as also applies to the high-anisotropy regime described in the following, we do not find a clear indication for this scenario.

C. High-anisotropy regime

We have obtained detailed susceptibility data in the strong-anisotropy regime as the system evolves toward the weakly coupled one-dimensional limit (Fig. 6). As found there, the strong decay of correlations between the effectively weakly coupled one-dimensional chains is already dominant, which manifests itself in a strong smearing of the magnetic susceptibility along k_y. As ξ is increased, the spectral weight of the susceptibility gets more and more reduced, while the fluctuation structure remains rather stable. We only observe reminiscences of c-AFM fluctuations smeared along k_y. From there, we do not find clear indication for a bi-spin liquid scenario suggested in the literature for that regime, where one magnetically disordered phase should be gapped while the other should be gapless.[26] A transition between those phases should manifest itself in the susceptibility by some jump in the spectral weight. In addition the bi-spin liquid scenario suggests no breaking of lattice symmetries, which appears to disagree with the c-AFM fluctuations which we find in the magnetically disordered strong anisotropy regime. In general, at large anisotropies energy scales involved in the coupling between the chains become so small that a caveat has to be given from the frequency discretization incorporated in the method, which sets a lower bound of energy scales to be resolvable. To rule out an artefact of this kind, for the anisotropy range considered by us, we varied the frequency mesh in the lower energy regime, and we found no notable change of our results. While this holds for the anisotropy regime considered, we cannot exclude different physical scenarios for even higher anisotropy.

V. CONCLUSION

In conclusion, we have used the pseudofermion functional renormalization group to study the different phases of the anisotropic triangular lattice. We find that upon variation of

the anisotropy parameter ξ, the system is divided into three distinct phases: Néel order, spiral order, and a disordered phase with c-AFM stripe fluctuations. We find evidence for a second-order transition between the first two and a first-order transition between the last two of these phases. The results give us confidence that our method is a suitable starting point to discuss various other problems in the field of frustrated magnetism.

ACKNOWLEDGMENTS

We thank P. Schmitteckert for his numerical support. We thank D. A. Abanin, B. A. Bernevig, A. Katanin, A. Läuchli, K. P. Schmidt, S. Sondhi, O. Tchernyshyov, S. Wessel, and, in particular, P. Wölfle for discussions. J.R. is supported by DFG-FOR 960. R.T. is supported by a Feodor Lynen Fellowship of the Humboldt Foundation and Alfred P. Sloan Foundation funds.

[1] G. Misguich and C. Lhuillier, in *Frustrated Spin Systems* (World Scientific, Singapore, 2004).
[2] A. W. Sandvik and J. Kurkijärvi, Phys. Rev. B **43**, 5950 (1991).
[3] S. R. White, Phys. Rev. Lett. **69**, 2863 (1992).
[4] U. Schollwöck, Rev. Mod. Phys. **77**, 259 (2005).
[5] D. J. J. Farnell and R. F. Bishop, in *Quantum Magnetism*, Vol. 645 of Lecture Notes in Physics (Springer-Verlag, Berlin, 2004).
[6] L. Capriotti, A. E. Trumper, and S. Sorella, Phys. Rev. Lett. **82**, 3899 (1999).
[7] D. Poilblanc, M. Mambrini, and D. Schwandt, Phys. Rev. B **81**, 180402(R) (2010).
[8] F. Wegner, Ann. Phys. (Leipzig) **3**, 77 (1994).
[9] F. Mila and K. P. Schmidt, e-print arXiv:1005.2495.
[10] S. R. White and A. L. Chernyshev, Phys. Rev. Lett. **99**, 127004 (2007).
[11] F. Verstraete, J. I. Cirac, and V. Murg, Adv. Phys. **57**, 143 (2008).
[12] G. Evenbly and G. Vidal, Phys. Rev. Lett. **102**, 180406 (2009).
[13] G. Evenbly and G. Vidal, Phys. Rev. Lett. **104**, 187203 (2010).
[14] J. Reuther and P. Wölfle, Phys. Rev. B **81**, 144410 (2010).
[15] R. Coldea, D. A. Tennant, A. M. Tsvelik, and Z. Tylczynski, Phys. Rev. Lett. **86**, 1335 (2001).
[16] Y. Shimizu, K. Miyagawa, K. Kanoda, M. Maesato, and G. Saito, Phys. Rev. Lett. **91**, 107001 (2003).
[17] T. Itou, A. Oyamada, S. Maegawa, M. Tamura, and R. Kato, Phys. Rev. B **77**, 104413 (2008).
[18] D. Heidarian, S. Sorella, and F. Becca, Phys. Rev. B **80**, 012404 (2009).
[19] M. Kohno, Phys. Rev. Lett. **103**, 197203 (2009).
[20] M. Q. Weng, D. N. Sheng, Z. Y. Weng, and R. J. Bursill, Phys. Rev. B **74**, 012407 (2006).
[21] J. Merino, R. H. McKenzie, J. B. Marston, and C. H. Chung, J. Phys. Condens. Matter **11**, 2965 (1999).
[22] S.-Q. Shen and F. C. Zhang, Phys. Rev. B **66**, 172407 (2002).
[23] R. F. Bishop, P. H. Y. Li, D. J. J. Farnell, and C. E. Campbell, Phys. Rev. B **79**, 174405 (2009).
[24] T. Pardini and R. R. P. Singh, Phys. Rev. B **77**, 214433 (2008).
[25] W. Zheng, R. H. McKenzie, and R. P. Singh, Phys. Rev. B **59**, 14367 (1999).
[26] S. Yunoki and S. Sorella, Phys. Rev. B **74**, 014408 (2006).
[27] O. A. Starykh and L. Balents, Phys. Rev. Lett. **98**, 077205 (2007).
[28] C. Wetterich, Phys. Lett. B **301**, 90 (1993).
[29] T. R. Morris, Int. J. Mod. Phys. A **9**, 2411 (1994).
[30] C. Honerkamp, M. Salmhofer, N. Furukawa, and T. M. Rice, Phys. Rev. B **63**, 035109 (2001).
[31] R. Hedden, V. Meden, T. Pruschke, and K. Schönhammer, J. Phys. Condes. Matter **16**, 5279 (2004).
[32] A. A. Katanin, Phys. Rev. B **70**, 115109 (2004).
[33] M. Salmhofer, C. Honerkamp, W. Metzner, and O. Lauscher, Prog. Theor. Phys. **112**, 943 (2004).
[34] P. W. Anderson, Phys. Rev. **86**, 694 (1952).
[35] J. Brinckmann and P. Wölfle, Phys. Rev. B **70**, 174445 (2004).
[36] I. Affleck and J. B. Marston, Phys. Rev. B **37**, 3774 (1988).
[37] J. B. Marston and I. Affleck, Phys. Rev. B **39**, 11538 (1989).